Experimental determination of the magnetic field spectrum in the Helically Symmetric Experiment using passing particle orbits

J. N. Talmadge, V. Sakaguchi, F. S. B. Anderson, D. T. Anderson, and A. F. Almagri

Citation: Physics of Plasmas **8**, 5165 (2001); doi: 10.1063/1.1415071
View online: http://dx.doi.org/10.1063/1.1415071
View Table of Contents: http://scitation.aip.org/content/aip/journal/pop/8/12?ver=pdfcov
Published by the AIP Publishing

Experimental determination of the magnetic field spectrum in the Helically Symmetric Experiment using passing particle orbits

J. N. Talmadge,[a] V. Sakaguchi, F. S. B. Anderson, D. T. Anderson, and A. F. Almagri
HSX Plasma Laboratory, Department of Electrical and Computer Engineering, University of Wisconsin, Madison, Wisconsin 53706

(Received 17 May 2001; accepted 12 July 2001)

The leading terms of the magnetic field spectrum for the Helically Symmetric Experiment [Fusion Technol. **27**, 273 (1995)] at low magnetic field are determined by analyzing the orbits of passing particles. The images produced by the intersection of electron orbits with a fluorescent mesh are recorded with a charge coupled device and transformed into magnetic coordinates using a neural network. To obtain the spectral components, the transformed orbits are then fit to an analytic expression that models the drift orbits of the electrons. The results confirm for the first time that quasihelical stellarators have a large effective transform that results in small excursions of particles from a magnetic surface. The drift orbits are also consistent with a very small toroidal curvature component in the spectrum. An external magnetic perturbation, nearly resonant with the transform, is shown to induce a large excursion of the particle orbit off a flux surface. © *2001 American Institute of Physics.* [DOI: 10.1063/1.1415071]

I. INTRODUCTION

Since the pioneering development of the HELIAS[1] (Helical Advanced Stellarators) approach, present-day advanced stellarators are designed to meet specific physics criteria with regard to equilibrium, stability and transport, among other requirements. These properties can be directly controlled by specification of the plasma boundary shape and the pressure and current (if present) profiles. Fast three-dimensional equilibrium solvers[2,3] coupled to nonlinear constrained optimization algorithms sift through the vast multidimensional parameter space to identify promising configurations. This task was aided considerably with the understanding by Boozer that the confinement depends on the spectrum in magnetic coordinates of the magnetic field magnitude $|B|$, not the components of B.[4] These advances were instrumental in allowing configurations to be developed that overcame one of the weaknesses of the conventional stellarator concept, namely the poor confinement of trapped particles at low collisionality due to the combination of toroidal and helical components of the spectrum. Such an optimization procedure was used to design the Wendelstein 7X stellarator.[5] Nührenberg and Zille[6] also showed that the neoclassical confinement properties of a stellarator could be made comparable to a tokamak, if not better, by optimizing the $|B|$ spectrum such that the toroidal curvature is minimized and only a single helical term is dominant. They termed this configuration quasi-helically symmetric because the symmetry was only with regard to the field magnitude. Subsequently, other advanced stellarators that seek to optimize the magnetic spectrum, such as the quasi-axisymmetric[7,8] and quasi-omnigeneous[9] stellarators, have also been identified.

The magnetic field spectrum in the straight field line, Boozer coordinate system is written as

$$\frac{B}{B_0} = \sum b_{nm} \cos(n\phi - m\theta), \tag{1}$$

where n is the toroidal mode number and m is the poloidal mode number. For a quasi-helically symmetric stellarator, the spectrum can be approximated with a single harmonic, $B/B_0 = b_{nm}\cos(n\phi - m\theta)$. Along a magnetic field line given by $\theta = \iota\phi$, where ι is the rotational transform, the dependence of the field on the toroidal coordinate ϕ is $B/B_0 = b_{nm}\cos[(n-m\iota)\phi]$. This is similar to the variation in the field for a tokamak with the substitution $\iota_{\text{eff}} = n - m\iota$. For the Helically Symmetric Experiment (HSX),[10,11] where $n=4$, $m=1$ and the rotational transform varies between 1.05 in the center and 1.12 at the edge, the effective transform is close to 3. Theoretically, the high effective transform is responsible for small drifts of passing particles from a flux surface, small banana widths for trapped particles, very low neoclassical transport for a stellarator, small plasma currents and a small Shafranov shift at finite beta.

It is desirable to find an experimental method for advanced stellarators to determine whether the expected magnetic field spectrum has been realized. Since the early days of the stellarator program, the vacuum magnetic surfaces have been mapped with a low-energy electron beam to determine whether the surfaces are well formed or if island structures detrimental to the plasma confinement might exist.[12] Such methods include the use of fluorescent screens,[13] fluorescent rods,[14] diode[15] and triode[16] emissive filaments, and tomographic[17] techniques. However, having well-formed magnetic surfaces, by themselves, does not guarantee that the magnetic field spectrum conforms to the optimized design goal. In this article, we present a method of determining the leading coefficients of the magnetic field spectrum by tracking the drift orbits of energetic electrons at several toroidal locations.

The disadvantage of this method is that it is not sensitive

[a]Electronic mail: talmadge@facstaff.wisc.edu

to $m=0$ modes in the spectrum which do not contribute to the drift of a circulating particle off a flux surface. The advantage of the method is that it is possible to find small magnetic spectral components that are nearly resonant with the transform. These modes can lead to very large excursions of particles from a flux surface. Mynick[18,19] has shown that such modes can have a much lower stochastic threshold for energetic particles than for the magnetic surfaces (see Figs. 4 and 5 in Ref. 18). On the other hand, the proper tailoring of such modes can be used for burn control and ash removal. The analysis of energetic passing particles in a stellarator can also be extremely important for optimizing the efficiency of tangential neutral beam injection (NBI).[20] In the Advanced Toroidal Facility (ATF), for example, measured neutron rates in certain magnetic configurations indicated an enhanced loss of energetic passing ions.[21]

The drift orbits of energetic passing electrons have been measured in both the Compact Auburn Torsatron[22,23] and in Heliotron DR[23] and shown to agree well with the analytic expression for particles that move in a tokamak-like field which includes only toroidal curvature, i.e., $n=0$, $m=1$. In general, stellarators contain a multiple of helical harmonics as well and in experiments such as in ATF the helical terms were believed to make a significant contribution to the drift orbit of energetic ions during tangential NBI.[21] For advanced stellarators, especially in HSX where the toroidal curvature term is minimal, the helical terms may be the dominant component in determining the drift orbits. In Sec. II we derive an approximate expression for the drift orbit of a passing particle in an arbitrary magnetic field with $v_\perp \sim 0$. Experimental results illustrating the method for determining the leading terms of the magnetic field spectrum are given in Sec. III. We illustrate in this section the usefulness of the approach presented here by demonstrating how a small, nearly resonant magnetic perturbation can have a sizable effect on the drift trajectory, while having minimal impact on the magnetic surfaces. Finally, Sec. IV includes some summarizing discussion.

II. PASSING PARTICLE ORBITS

In this section we derive an approximate analytic expression for the motion of a passing particle in an arbitrary magnetic field. Assuming that the magnetic moment $\mu=0$, the parallel velocity $v_\parallel$ is a constant. In a curl-free magnetic field, the guiding center equations in the Boozer coordinates, r, θ, ϕ, are then given by[24]

$$B_0 r \frac{dr}{dt} = -\frac{M v_\parallel^2}{eB}\frac{dB}{d\theta}, \tag{2a}$$

$$\frac{d\theta}{dt} = \frac{\iota B v_\parallel}{g} + \frac{M v_\parallel^2}{eB}\frac{1}{B_0 r}\frac{dB}{dr}, \tag{2b}$$

$$\frac{d\phi}{dt} = \frac{B v_\parallel}{g}. \tag{2c}$$

In the equations above, M is the particle mass, g is related to the poloidal current outside a flux surface and r is a flux surface variable given by $\psi = B_0 r^2/2$. B_0 is the magnetic field on the magnetic axis and $2\pi\psi$ is the toroidal flux. Passing particle orbits are dependent on the magnetic field spectrum through the $dB/d\theta$ term in Eq. (2a). We assume that for small drifts off the flux surface, the rotational transform and the spectral components b_{nm} in Eq. (1) are independent of the flux coordinate r. We also ignore, for the moment, the term dependent on the radial derivative of the magnetic field on the right-hand side of Eq. (2b). The effect of this term will be considered in the next section. With these assumptions a simple expression for the particle orbit can be derived,

$$r^2 = r_0^2 + \frac{2 M v_\parallel g}{e B_0^2} \sum b_{nm} \frac{m}{n - m\iota} [\cos(n\phi - m\theta) - \delta_{nm}]. \tag{3}$$

When a particle is launched at initial Boozer angles ϕ_0 and θ_0, the constants $\delta_{nm} = \cos(n\phi_0 - m\theta_0)$ force the radial coordinate r to be equal to r_0, the home flux surface. From the equation above it is apparent that $m=0$ modes do not contribute to the radial drift of a passing particle. However, for spectral components b_{nm} such that $\iota \sim n/m$, even small amplitude terms can result in a large drift of a particle off a flux surface. Because of the dependence of the particle orbits on the b_{nm} spectral coefficients, Eq. (3) suggests that given the orbits at multiple poloidal and toroidal angles, it may be possible to reconstruct the leading terms of the magnetic field spectrum.

For a conventional tokamak with $n=0$ and $m=1$, the toroidal curvature term b_{01} is equal to r/R and the Boozer g factor is given by $B_0 R$, where R is the major radius. For $r \sim r_0$, Eq. (3) then reduces to the standard expression for the shift of the particle center from the magnetic axis, $\delta r = M v_\parallel / e B_0 \iota$.[25] For a quasi-helically symmetric stellarator like HSX, with a dominant mode $n=4$ and $m=1$, the displacement of the drift orbit is smaller by a factor of $(n - m\iota)/\iota$ than a tokamak with the same rotational transform. Figure 1 illustrates how the spatial scale over which $dB/d\theta$ changes sign is much shorter for the quasi-helically symmetric stellarator than for the tokamak, thereby allowing for a smaller excursion of the particle orbit from the magnetic surface. The figure also illustrates the physical origin of the resonance in Eq. (3). As the magnetic field line becomes more and more parallel to a constant $|B|$ contour, i.e., $\iota \sim n/m$, then $dB/d\theta$ changes sign over increasingly large distances. For a tokamak this occurs when $\iota \sim 0$. Finally, one can conclude that for a particle launched at $\theta=0$, $\phi=0$, the direction of the particle drift in the radial direction, i.e., inside or outside the home flux surface, will be opposite for the quasi-helically symmetric stellarator compared to a device in which only toroidal curvature exists. This is due to the opposite sign, at this location, of the $B\times\nabla B$ drift for the two cases.

III. EXPERIMENTAL DETERMINATION OF THE FIELD SPECTRUM

The drift orbits of passing electrons are measured in HSX using an electron gun, fluorescent mesh and a charge coupled device (CCD) camera. The mesh itself is made of 0.076 mm copper wire with 3 mm grid spacing and a fluo-

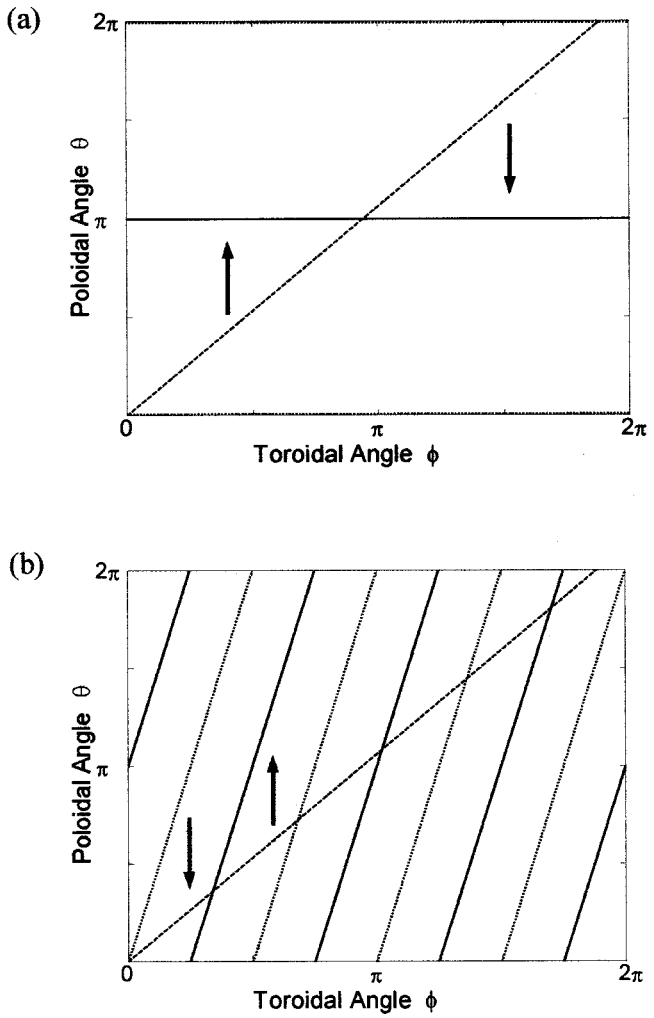

FIG. 1. Contours of constant $|B|$ and a magnetic field line with a rotational transform $\iota = 1.06$. The solid lines are the maxima of the field strength, the dotted lines are the minima and the dashed curve is the field line. The vertical arrows illustrate the direction of increasing $|B|$ in the poloidal direction. Shown are (a) tokamak-like configuration with a magnetic field spectrum consisting of only an $n=0$, $m=1$ mode and (b) HSX-like configuration with only an $n=4$, $m=1$ mode.

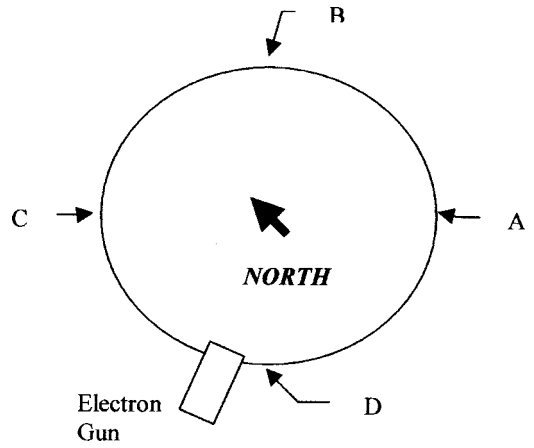

FIG. 2. Experimental set-up showing orientation of the box ports with respect to the electron gun. Drift orbits are detected with a fluorescent mesh at ports B, C and D.

rescent coating. Twenty-two light emitting diodes are mounted on the frame surrounding the mesh and are used to provide an absolute reference mark. A high-sensitivity CCD camera records the images produced when the electrons strike the mesh. A calibration grid is used to correct for optical and geometric distortions of the image. HSX is a four field period device with 12 coils per field period. Figure 2 shows the experimental set-up. Between each of the field periods are large diagnostic box ports separated by 90° and labeled A, B, C and D in the figure. The electron gun is fixed in position near the location of box port D. The energy of the electrons could be varied up to 450 eV. A stepper motor moves the electron gun in the radial direction so that a family of drift surfaces can be recorded.

The number of spectral components that can be determined by analyzing drift orbits is limited by the number of toroidal planes at which the fluorescent mesh can be placed. Due to access restrictions, we were constrained to put the mesh into three of the large box ports: D, C and B located $-7°$, 83° and 173° from the electron gun. Because of the very small drift excursion of particles in quasi-helically symmetric stellarators, it was necessary to lower the magnetic field to 90 G to observe the deviation of the electron orbits from a flux surface. Drift orbits were then compared at 50 and 450 eV. Figure 3 shows the orbit shift of the higher energy particle with respect to the lower one. The contrast for the images has been enhanced to help illustrate the orbit shift.

The orbits shown in Fig. 3 have been corrected for image distortion. However, to use Eq. (3) to obtain the magnetic field spectrum, the images must be converted into the appropriate Boozer coordinates.[24,26] The contravariant representation of the field is given by, $B=\nabla\psi\times\nabla\theta_0$, and for a curl-free field is given in the covariant representation as $B=\nabla\chi$. A point in space is then described by the coordinate ψ, which labels the flux surfaces, the coordinate θ_0, an angle which labels the field lines, and $\chi=\int Bdl$, which is related to the distance along the field line. The Boozer poloidal and toroidal angles, θ and ϕ, are then defined by

$$\chi = g(\psi)\phi + I(\psi)\theta,$$
$$\theta_0 = \theta - \iota\phi. \tag{4}$$

The quantity $I(\psi)$, related to the total toroidal current within a flux surface, is equal to zero for the current-free HSX experiment. The Boozer toroidal angle $\phi=(1/g)\int Bdl$ was determined from a numerical calculation to be within a few degrees of the standard cylindrical toroidal angle in the lab frame of reference.

Experimentally, we map the vacuum surfaces at low energy and identify N successive passes of the beam. For each pass the local transform is given $\iota_N=\Delta\theta_L/\Delta\phi_L$, where $\Delta\theta_L$ and $\Delta\phi_L$ are the total poloidal and toroidal angles the beam has traversed for that pass in the lab coordinate system. The extrapolation of ι_N as $N\to\infty$ yields an estimate of the flux surface transform ι. For each successive pass of the beam the Boozer poloidal angle at that location is then determined by $\theta=\iota\phi$ where we used the cylindrical coordinate

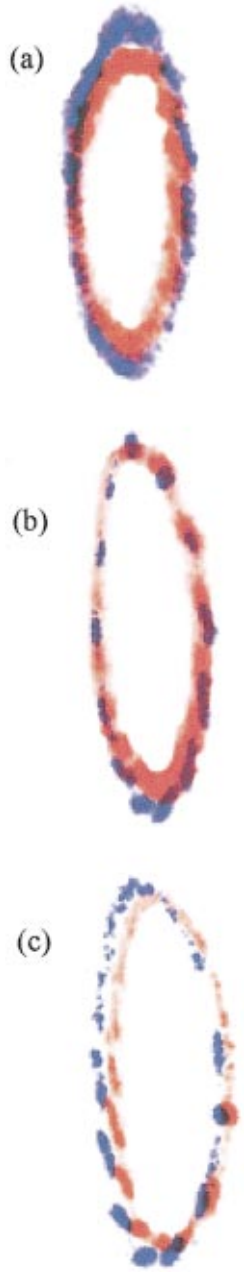

FIG. 3. (Color) High energy (450 eV, red) and low energy (50 eV, blue) electron orbits at (a) box port D, located −7° toroidally from the electron gun, (b) box port C (83°), and (c) box port B (173°). The outboard side is to the right.

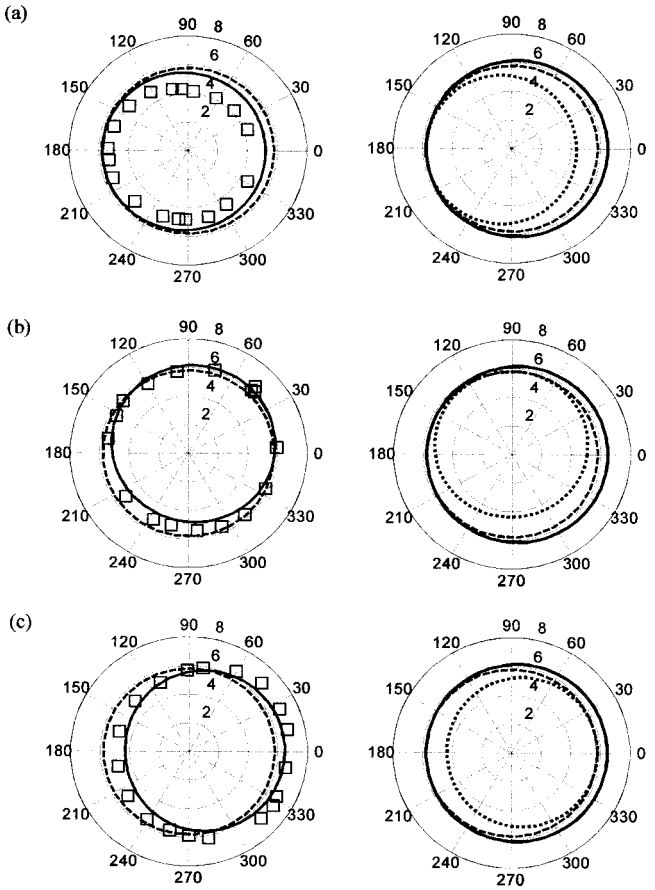

FIG. 4. Experimental data (squares) mapped from Fig. 3 into magnetic coordinates and the best fit (solid line) of Eq. (3) to the data. The dashed line is the starting flux surface for the electron orbit. To the right of each graph are the individual contributions of the b_{11} mode (dotted) and the b_{41} (solid) to the drift orbit. Shown are the orbits for (a) box port D (b) box port C and (c) box port B. The outboard side is to the right.

for the Boozer toroidal angle. To obtain the flux surface variable r, the area enclosed by each flux surface is used instead of the toroidal flux. The error introduced by this approximation is on the order of a few percent.

We use a neural network[27] to generalize the mapping from lab to Boozer coordinates. Neural networks have been used before for rapid mapping of complex stellarator geometry into the magnetic flux coordinate ψ.[28] Here, however, we include in the mapping the Boozer poloidal coordinate. Also we rely solely on the experimental data for the mapping, rather than numerical equilibrium codes. The drift orbits of low-energy electrons at 50 eV are used as approximations to the magnetic surfaces. Typically we use four such surfaces that span the radial extent of the high-energy orbit and about 13 poloidal angles for each surface, at each of the three toroidal locations. The network used is the standard multilayer perceptron with only one hidden layer. Typically one would use a network that has two inputs, the x and y coordinates of the beam passes with respect to the frame of the fluorescent mesh, and two outputs, the Boozer poloidal angle and radial coordinate. However, to overcome the mapping difficulties when the angle jumps between 2π and 0, an alternative approach was used. Data on the outboard side of the torus (corresponding to a Boozer poloidal angle of zero) were mapped from $-\pi$ to π, while data on the inboard side were mapped from 0 to 2π. To verify that the mapping was indeed an adequate generalization of the training data and to avoid over fitting, data on two flux surfaces that the network was not trained on were used as testing data.

Figure 4 shows the transformation of the high-energy electron orbit into Boozer coordinates for the three toroidal locations. Also shown is the best fit of Eq. (3) to the data. There are two components to the spectrum that can be resolved using this method; the normal dominant helical term $b_{41}=-0.051$ and an additional mode $b_{11}=0.0023$. If, instead, the coupled differential equations of Eq. (2) are solved, including the dB/dr term that was omitted to derive

TABLE I. Numerical calculation of the magnetic field spectrum in HSX at 90 G including earth's magnetic field.

(n,m)	Amplitude
(4,1)	−0.072 62
(3,0)	0.025 24
(4,0)	−0.011 82
(1,1)	0.003 56
(4,2)	−0.002 75

Eq. (3), the spectral components are $b_{41}=-0.045$ and $b_{11}=0.0023$. The b_{11} term is nearly resonant with the rotational transform in HSX, which is just above one. Hence, this mode dominates the actual drift of the particle even though it is over an order of magnitude smaller than the leading term. Also shown in Fig. 4 are the individual contributions of each of the modes. Because of the symmetric placement of the fluorescent mesh at each of the three large box ports, the contribution of the b_{41} mode to the orbit is the same for all three cases. However, the component of the orbit drift due to the b_{11} mode rotates by 90° in going from one box port to the next.

The coefficients obtained above are an underestimate of the amplitudes of the modes because, at 50 eV, the electrons used to perform the coordinate mapping are still slightly shifted from the flux surfaces. Extrapolating the mapping down to zero energy and taking into account the errors in the beam localization, image restoration, coordinate transformation and other experimental errors, the spectral components are then $b_{41}=-0.077\pm0.008$ and $b_{11}=0.0034\pm0.0004$.

To compare these amplitudes to the theoretical values, we calculate the Boozer spectrum for HSX using an ideal finite-size coil representation. A numerical model of the earth's field,[29] evaluated at the location of the laboratory, is included in the calculation. At nominal 1 T operation the earth's field has a negligible effect on the spectrum and the leading symmetry-breaking term for the quasi-helical configuration in HSX is the $n=4$, $m=2$ mode with an amplitude less than 5% of the main $n=4$, $m=1$ term. However, at a magnetic field of 90 G, the earth's field breaks the quasi-helical symmetry. A listing of the first five components of the magnetic field spectrum is given in Table I. The largest symmetry-breaking term is now the [3,0] with an amplitude roughly $\frac{1}{3}$ that of the [4,1] term. Also of sizable magnitude is the [4,0] term. Note that from Eq. (3), neither of these terms has an effect on the radial excursion of a passing particle. For the top two $m\neq0$ terms, the model calculation yields $b_{41}=-0.072\,62$ and $b_{11}=0.003\,56$. The phase of the [1,1] mode in the calculation differs by 45° compared to the data.

IV. DISCUSSION AND CONCLUSIONS

The distinguishing characteristic of the quasi-helically symmetric stellarator is the near-absence of toroidal curvature in the magnetic field spectrum. The placement of the fluorescent mesh at three box ports that are separated by one field period does not allow for an unambiguous measurement of the toroidal curvature. The main helical mode in HSX, the b_{41} term, is indistinguishable from a b_{01} term or a b_{81} term without additional data. However, the passing particle orbits shown in Figs. 3 and 4 are not consistent with the negative (i.e., low field on the outboard side) toroidal curvature spectral component present in other toroidal devices. This can be seen from Fig. 1, which shows for a particle launched near a toroidal angle of 0° the $B\times\nabla B$ drift is in opposite directions for HSX compared to a conventional tokamak. This is illustrated in Fig. 5 and shows the drift orbit of a passing particle in a magnetic field with only toroidal curvature, but with an amplitude equal to that of the b_{41} term shown in Fig. 4(c). For consistency, the mode amplitude is constant as a function of radius. For Fig. 5, the particle orbit on the outboard side is inside the home flux surface, while for Fig. 4(c) the experimental data shows the orbit is outside the flux surface. It should also be noted that the magnitude of the orbit excursion for the b_{41} term is on the order of $\frac{1}{3}$ that due to the b_{01} term due to the $n-m\iota$ factor in Eq. (3).

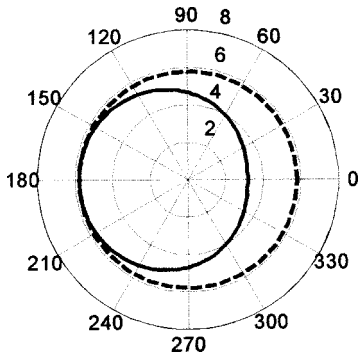

FIG. 5. Orbit of a passing electron in a magnetic field with only toroidal curvature. The outboard side is to the right.

In this article we have shown that the leading $m\neq0$ terms of the magnetic field spectrum in HSX can be determined by analyzing the orbits of passing particles. Specifically, this method is very sensitive in picking up nearly resonant small-amplitude spectral components that can have a strong effect on the drift orbit. At very low magnetic field, this occurs in HSX due to a [1,1] mode from the earth's magnetic field that is inconsequential at the normal operating field of 1 T. There exists another advantage of using passing particle orbits to determine the leading spectral components. The method can also be used to investigate whether a specific component of the spectrum is intrinsic to the confinement coil set or whether the perturbation is due to an outside source. For an intrinsic component, a reversal of the magnetic field shifts the orbit to the opposite side of the home flux surface, i.e., orbits outside the surface will now be inside and vice versa. However, for an external perturbation a reversal of the field also reverses the sign of the mode amplitude so that the net $B\times\nabla B$ drift is unaffected. This is clearly seen in HSX at box port B [see Fig. 3(c) for example] where the deviation of the orbit on the left is due to the [1,1] mode, while the deviation of the orbit on the right is due to the [4,1] mode. The deviation of the higher energy orbit from the lower energy one is shown in Fig. 6 when the direction of the magnetic field is reversed from that in Fig. 3. For the [4,1] mode the higher energy orbit is now inside the lower energy one, the opposite of what is seen in Fig. 3(c). However, for

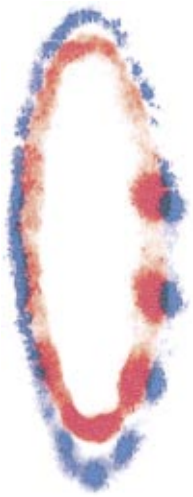

FIG. 6. (Color) High energy (450 eV, red) and low energy (50 eV, blue) electron orbits at box port B, but with the direction of the magnetic field reversed from Fig. 3(c). The outboard side is to the right.

the [1,1] mode due to the earth's magnetic field, a reversal of the magnetic field direction still leaves the relative positions of the high and low energy orbits unperturbed. This result confirms that the nearly resonant perturbation observed in the drift orbits is due to a perturbation of the HSX magnetic field that is external to the modular coils.

To summarize, we have demonstrated a method by which advanced stellarators can determine the leading $m \neq 0$ terms of the magnetic field spectrum. The method is especially useful for picking out the nearly resonant spectral components and can be used to determine whether such components are due to errors in the coil set or to some external perturbation. In addition, we have shown that the drift orbit excursions in quasi-helically symmetric stellarators are reduced compared to the equivalent tokamak. Finally, we have shown that for HSX, it is possible to build a toroidal stellarator with very little toroidal curvature.

ACKNOWLEDGMENT

This work is supported by the United States Department of Energy under Grant No. DE-FG02-93ER54222.

[1] J. Nührenberg and R. Zille, Phys. Lett. A **114**, 129 (1986).
[2] S. P. Hirshman and J. C. Whitson, Phys. Fluids **26**, 3553 (1983).
[3] M. Taylor, J. Comput. Phys. **110**, 407 (1994).
[4] A. H. Boozer, Phys. Fluids **26**, 496 (1983).
[5] C. Beidler, G. Grieger, F. Hernegger *et al.*, Fusion Technol. **17**, 148 (1990).
[6] J. Nührenberg and R. Zille, Phys. Lett. A **129**, 113 (1988).
[7] J. Nührenberg, W. Lotz, and S. Gori, *Theory of Fusion Plasmas*, Varenna, 1994 (Editrice Compositori, Bologna, 1994), p. 3.
[8] P. R. Garabedian, Phys. Plasmas **4**, 1617 (1997).
[9] S. P. Hirshman, D. A. Spong, J. C. Whitson *et al.*, Phys. Plasmas **6**, 1858 (1999).
[10] F. S. B. Anderson, A. F. Almagri, D. T. Anderson, P. G. Matthews, J. N. Talmadge, and J. L. Shohet, Fusion Technol. **27**, 273 (1995).
[11] D. T. Anderson, A. F. Almagri, F. S. B. Anderson *et al.*, J. Plasma Fusion Res. **1**, 49 (1998).
[12] R. M. Sinclair, J. C. Hosea, and G. V. Sheffield, Appl. Phys. Lett. **17**, 92 (1970).
[13] G. J. Hartwell, R. F. Gandy, M. A. Henderson *et al.*, Rev. Sci. Instrum. **59**, 460 (1988).
[14] H. Hailer, J. Massig, F. Schuler, K. Schworer, and H. Zwicker, in *Proceedings of the 14th European Conference on Controlled Fusion and Plasma Physics*, Madrid, 1987 (European Physical Society, Geneva, 1987), Vol. 11D, Part 1, p. 423.
[15] R. F. Gandy, M. A. Henderson, J. D. Hanson, G. J. Hartwell, and D. G. Swanson, Rev. Sci. Instrum. **58**, 509 (1987).
[16] A. G. Dikii, V. M. Zalkind, G. G. Lesnyakov *et al.*, Sov. J. Plasma Phys. **14**, 160 (1988).
[17] B. D. Blackwell, J. Howard, and R. B. Tumlos, Rev. Sci. Instrum. **63**, 4725 (1992).
[18] H. E. Mynick, Phys. Fluids B **5**, 1471 (1993).
[19] H. E. Mynick, Phys. Fluids B **5**, 2460 (1993).
[20] M. S. Smirnova, Phys. Plasmas **4**, 2584 (1997).
[21] M. R. Wade, C. E. Thomas, R. J. Colchin, J. A. Rome, A. C. England, and R. H. Fowler, Nucl. Fusion **35**, 1029 (1995).
[22] R. F. Gandy, H. Lin, G. J. Hartwell, S. F. Knowlton, S. Morimoto, and D. Pritchard, Phys. Plasmas **2**, 1270 (1995).
[23] S. Morimoto, T. Obiki, H. Lin, G. Hartwell, T. A. Schneider, S. F. Knowlton, and R. F. Gandy, Fusion Technol. **27**, 202 (1995).
[24] A. H. Boozer, Phys. Fluids **23**, 904 (1980).
[25] K. Miyamoto, *Plasma Physics for Nuclear Fusion* (MIT, Cambridge, MA, 1976).
[26] A. H. Boozer and G. Kuo-Petravic, Phys. Fluids **24**, 851 (1981).
[27] Neural Network Toolbox, distributed by The Math Works Inc., Natick, MA.
[28] V. Tribaldos and B. P. Van Milligen, Rev. Sci. Instrum. **68**, 931 (1997).
[29] Geomagix, written by John Quinn of the US Geological Survey, distributed by Interpex Limited, Golden, CO.